Numerical Investigation of Free Convection between Two Vertical Coaxial Cylinders

THOMAS H. SCHWAB and KENNETH J. DE WITT

University of Toledo, Toledo, Ohio

Free convection between two vertical coaxial cylinders was studied by solving the governing transport equations as an initial-value problem. The coupled, nonlinear, partial differential equations were converted into a set of difference equations by use of an alternating-direction implicit finite-difference numerical scheme. Twenty-four different combinations of Prandtl and Grashof numbers, and height to annular spacing ratios were used to characterize the problem. The results are presented primarily in the form of contour maps for the steady-state isotherms and streamlines.

For Rayleigh numbers greater than 5×10^3, a fully developed boundary-layer flow was found to exist in the cavity. The interior region of the annulus was found to be thermally stratified and to possess a nearly uniform vertical temperature gradient, with a unicellular flow pattern being generated.

With Rayleigh numbers of 5×10^4 and greater, it was found that the flow patterns could not be properly described with a grid spacing of 1/10. The variation of the steady-state mean Nusselt number with Prandtl and Rayleigh numbers and with geometric ratios was also investigated.

Recent advances in heat transfer and fluid mechanics, together with the development of large digital computers, have made feasible the study of many natural phenomena of great practical importance. A case in point is the analysis of the cavity problem—free convection of a fluid in an annular container whose inner and outer walls are maintained at different uniform temperatures. The hydrodynamic and heat transfer processes, which are coupled for this system, can be described by the conservation principles of mathematical physics; namely, the conservation of mass, momentum, and energy.

The purpose of this study was to investigate steady free convection of a Boussinesq fluid between two closed, vertical, coaxial cylinders by numerical finite-difference techniques.

PREVIOUS WORK

Hellums (*8*) in 1960 was the first to solve two free convection problems by finite-difference techniques. He obtained solutions for convection from a heated vertical plate and for an infinitely long horizontal cylinder.

Many finite-difference solutions of free convection problems followed. Numerical studies of long, horizontal, rectangular enclosures subject to lateral heating are found in the works of Wilkes (*16*), Elder (*6*), and Noble (*11*). Deardorff (*4*), Fromm (*7*), and Samuels (*13*) made detailed studies for the case where the fluid is heated from below.

Numerical studies of free convection in long, horizontal, cylindrical annuli are found in the works of Lemlich and Crawford (*9*), Liu *et al.* (*10*), and Abbott (*1*). Numerical solutions to the problem of thermal convection in a rotating fluid annulus whose vertical walls are maintained at different uniform temperatures is curently receiving much attention. Axisymmetric flow regimes have been studied by Piacsek (*12*), Samuels (*14*), and Williams (*17, 18*).

This paper considers the axisymmetric flow regime without rotation and with only the Boussinesq approximations being made to the governing equations.

MATHEMATICAL FORMULATION OF THE PROBLEM

Two-dimensional axisymmetric motion of a Boussinesq fluid initially at rest and at a uniform temperature is as-

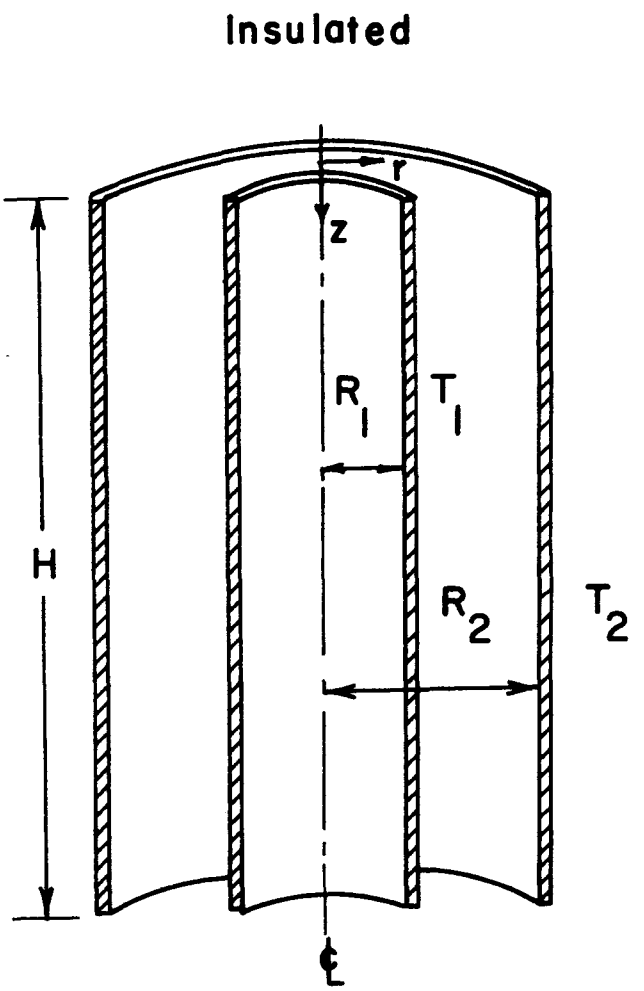

Fig. 1. Closed vertical annular container.

sumed in the mathematical model for the system shown in Figure 1. The vertical cylindrical surfaces are considered to be perfect conductors of heat, the inner wall being hotter than the outer wall. The initial uniform fluid temperature T_0 is taken as the mean of the two vertical wall temperatures. The top and bottom surfaces of the container are considered to be perfect insulators, and all bounding surfaces are motionless and rigid.

The appropriate equations of continuity, motion, and energy in terms of dimensionless variables are

$$\frac{\partial U}{\partial \xi} + \frac{U}{\xi} + \frac{\partial V}{\partial \eta} = 0 \tag{1}$$

$$\frac{\partial U}{\partial \tau} + \frac{U\partial U}{\partial \xi} + \frac{V\partial U}{\partial \eta} = -\frac{\partial P}{\partial \xi} + \frac{\partial^2 U}{\partial \xi^2} + \frac{1}{\xi}\frac{\partial U}{\partial \xi} - \frac{U}{\xi^2} + \frac{\partial^2 U}{\partial \eta^2} \tag{2}$$

$$\frac{\partial V}{\partial \tau} + \frac{U\partial V}{\partial \xi} + \frac{V\partial V}{\partial \eta} = -\frac{\partial P}{\partial \eta} - N_{Gr}\theta + \frac{\partial^2 V}{\partial \xi^2} + \frac{1}{\xi}\frac{\partial V}{\partial \xi} + \frac{\partial^2 V}{\partial \eta^2} \tag{3}$$

$$\frac{\partial \theta}{\partial \tau} + \frac{U\partial \theta}{\partial \xi} + \frac{V\partial \theta}{\partial \eta} = \frac{1}{N_{Pr}}\left(\frac{\partial^2 \theta}{\partial \xi^2} + \frac{1}{\xi}\frac{\partial \theta}{\partial \xi} + \frac{\partial^2 \theta}{\partial \eta^2}\right) \tag{4}$$

The initial and boundary conditions take the form:

Time	Surface	Thermal Conditions	Kinematic Conditions
$\tau = 0$		$\theta = \tilde{\theta}$	$U = V = 0$
$\tau > 0$	$\xi = R_1/(R_2 - R_1)$	$\theta = +1$	$U = V = 0$
	$\xi = R_2/(R_2 - R_1)$	$\theta = -1$	$U = V = 0$
	$\eta = 0$	$\frac{\partial \theta}{\partial \eta} = 0$	$U = V = 0$
	$\eta = H/(R_2 - R_1)$	$\frac{\partial \theta}{\partial \eta} = 0$	$U = V = 0$

Equations (2) and (3) may be combined through elimination of the pressure terms to yield a vorticity transport equation,

$$\frac{\partial \omega}{\partial \tau} + \frac{U\partial \omega}{\partial \xi} + \frac{V\partial \omega}{\partial \eta} - \frac{U\omega}{\xi} = N_{Gr}\frac{\partial \theta}{\partial \xi} + \frac{\partial^2 \omega}{\partial \xi^2} + \frac{1}{\xi}\frac{\partial \omega}{\partial \xi} - \frac{\omega}{\xi^2} + \frac{\partial^2 \omega}{\partial \eta^2} \tag{5}$$

where the azimuthal component of the vorticity is given by

$$\omega = \frac{\partial U}{\partial \eta} - \frac{\partial V}{\partial \xi} \tag{6}$$

The stream function $\Psi = \Psi(\xi, \eta)$ is introduced by defining the velocity components in terms of derivatives of Ψ so that the equation of continuity is identically satisfied:

$$U = \frac{1}{\xi}\frac{\partial \Psi}{\partial \eta} \quad ; \quad V = -\frac{1}{\xi}\frac{\partial \Psi}{\partial \xi} \tag{7}$$

The stream function is found to obey a Poisson type of equation given by

$$\omega\xi = \frac{\partial^2 \Psi}{\partial \xi^2} - \frac{1}{\xi}\frac{\partial \Psi}{\partial \xi} + \frac{\partial^2 \Psi}{\partial \eta^2} \tag{8}$$

The nonslip hydrodynamic boundary conditions for a motionless rigid surface require that both the normal and tangential velocity components vanish at a surface. These conditions expressed in terms of the stream function and vorticity yield

$$\Psi = \frac{\partial \Psi}{\partial n} = 0 \quad ; \quad \omega = \frac{1}{\xi_s}\frac{\partial^2 \Psi}{\partial n^2} \tag{9}$$

where $\partial/\partial n$ represents the normal derivative to the surface and ξ_s is the value of ξ appropriate to the surface.

The final equation needed to characterize the problem defines the mean Nusselt number and is given by

$$\overline{N_{Nu}} = -\frac{(R_2 - R_1)}{2H}\int_0^{H/(R_2-R_1)} \left(\frac{\partial \theta}{\partial \xi}\right)_{\xi = R_1/(R_2-R_1)} d\eta \tag{10}$$

Thus, a formal mathematical statement of the problem is given by Equations (4), (5), (7), (8), and (10), along with the initial and boundary conditions.

FINITE-DIFFERENCE FORMULATION OF THE PROBLEM

An analytic solution cannot be found for a set of equations of the complexity of those characterizing the cavity problem, and thus they must be integrated numerically by finite-difference techniques.

A two-dimensional version of the generalized alternating-direction implicit (ADI) scheme introduced by Brian (3) was used to advance the vorticity and energy equations across a single time step. The set of difference equations obtained (15) were solved by tridiagonal matrix inversion.

In order to avoid solving the elliptic stream function equation by either successive over-relaxation or by an ADI technique using a sequence of iteration parameters as developed by Douglas (5), Equation (8) was formulated as an unsteady equation

$$\frac{\partial \Psi}{\partial \tau} = \frac{\partial^2 \Psi}{\partial \xi^2} - \frac{1}{\xi}\frac{\partial \Psi}{\partial \xi} + \frac{\partial^2 \Psi}{\partial \eta^2} - \omega\xi \tag{11}$$

This is a somewhat artificial equation in that it can be derived only in part; however, constructing it in this manner allows a single constant iteration parameter to be used for the stream function iteration. This technique has proved to be successful in the work of Samuels (13, 14).

Four-point, central-difference approximations were used to evaluate the velocity components for grid points not adjacent to a boundary, whereas four-point noncentral approximations were used for grid points adjacent to a boundary. A symmetric, second-order correct approximation was used to evaluate the wall vorticities, and a third-order, four-point formula was used in calculating $\overline{N_{Nu}}$.

For a given vorticity field, Equation (11) is solved until the stream function is invariant in time. This is termed the "inner" iteration.

The velocity components and wall vorticities must be expressed in terms of the stream function and thus can be evaluated at the old or new level of time or at the midpoint of two time steps. In this study, these quantities were evaluated at the new level of time and, although this necessitates executing several iterations around each time step, the likelihood of generating boundary-induced instabilities is considerably reduced. Starting with the old values of the velocities and wall vorticities, several iterations were performed for the same point in problem time

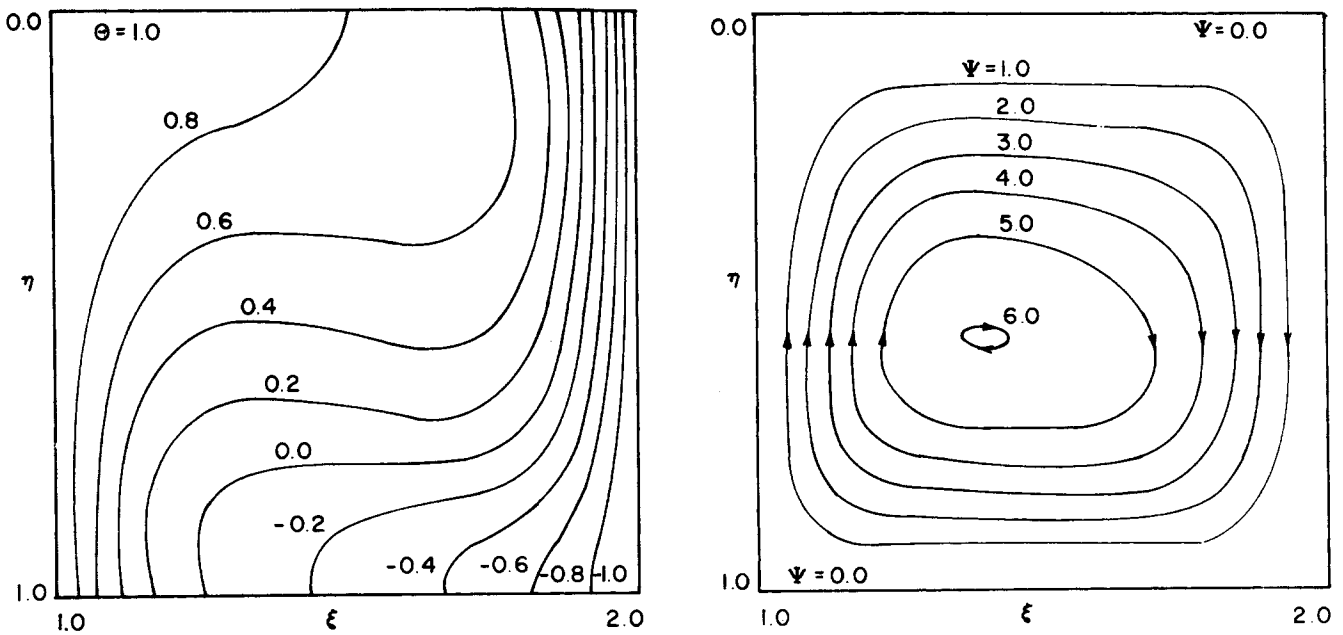

Fig. 2. Steady state isotherms and streamlines—$H/(R_2 - R_1) = 1.0$; $N_{PR} = 1.0$; $N_{GR} = 10{,}000$; $\Delta\xi = \Delta\eta = 1/10$.

until the vorticity field agreed with its previous approximation to within a specified constant. This is termed the "outer" iteration, and thus several inner and outer iterations must be performed at each time step before the solution is advanced to the next point in time.

RESULTS AND CONCLUSIONS

The difference equations of this study were solved on an IBM 360 Model 50 digital computer. The solutions are presented primarily in the form of contour maps for the steady-state isotherms and streamlines. The twenty-four different cases which were studied are summarized in Table 1.

Time Increments—Boundary-Induced Instability

It has been shown by Noble that serious stability limitations are known to exist when solving the vorticity transport equation as an initial-value problem using ADI numerical methods. The inability to describe properly the nonslip hydrodynamic boundary conditions in terms of the vorticity leads to a stability-imposed limitation on the size of the time step used to advance the numerical solutions. It was found that boundary-generated instabilities could be avoided by using the time increments shown in Table 1 and by using the method of solution outlined earlier.

It is desirable to find the optimum time step compatible with numerical stability and the total computer time needed to reach steady state. Approximate times in hours starting from conduction initial conditions ranged from ¾ hr. for an 11 × 11 grid to 4½ hr. for a 21 × 21 grid. Starting from the steady-state solution of a previous calculation, an average of 300 to 400 time increments was needed to reach steady state with a new set of parameters.

Effect of Grid Spacing on Numerical Solutions

Convergence of computed results as a function of grid spacing is one of the best tests for establishing the validity of numerical solutions to partial differential equations. For values of N_{Gr} below 5×10^4, a grid spacing of 1/10 was found to give an adequate representation of the isotherm and streamline contours. A comparison of Figures 2 and 3 substantiates this fact.

As convective strength builds in the annulus, thermal and hydrodynamic boundary-layer formation on the vertical walls of the enclosure imposes a restriction on the size of the space increments required to describe properly the flow patterns that exist in the annulus. Numerical experiments indicate that grid spacings of 1/20 or smaller are needed for $N_{Gr} \geq 5 \times 10^4$. Figure 4 represents the results of one of these experiments. This is to be contrasted with Noble's results for free convection in a square cavity where the vertical boundary layer formation did not become critical until N_{Gr} reached 10^6.

Table 1. Summary of Numerical Experiments

$\Delta\tau$	$H/(R_2 - R_1)$	$\Delta\xi$	$\Delta\eta$	N_{Pr}	N_{Gr}	N_{Ra}	$N_{\overline{Nu}}$
0.001 & 0.002	1.0	0.10	0.10	0.73	3,000	2,190	3.14
0.001 & 0.002	1.0	0.10	0.10	0.73	5,000	3,650	3.86
0.001 & 0.002	1.0	0.10	0.10	0.73	10,000	7,300	5.24
0.001 & 0.002	1.0	0.10	0.10	0.73	15,000	10,950	6.35
0.001 & 0.002	1.0	0.10	0.10	0.73	20,000	14,600	7.29
0.001 & 0.005	1.0	0.10	0.10	1.00	3,000	3,000	3.58
0.001 & 0.005	1.0	0.10	0.10	1.00	5,000	5,000	4.46
0.001 & 0.005	1.0	0.10	0.10	1.00	7,000	7,000	5.20
0.001 & 0.005	1.0	0.10	0.10	1.00	10,000	10,000	6.17
0.001 & 0.005	1.0	0.10	0.10	1.00	15,000	15,000	7.52
0.001 & 0.005	1.0	0.10	0.10	1.00	20,000	20,000	8.65
0.001	1.0	0.10	0.10	1.00	50,000	50,000	12.30
0.001	0.5	0.05	0.05	1.00	5,000	5,000	3.10
0.001 & 0.005	2.0	0.10	0.10	1.00	5,000	5,000	4.50
0.001 & 0.005	3.0	0.10	0.10	1.00	5,000	5,000	4.22
0.001	1.0	0.05	0.05	1.00	10,000	10,000	4.74
0.001	1.0	0.05	0.05	1.00	50,000	50,000	8.77
0.010	1.0	0.10	0.10	7.00	300	2,100	3.11
0.010	1.0	0.10	0.10	7.00	500	3,500	3.85
0.010	1.0	0.10	0.10	7.00	1,000	7,000	5.30
0.010	1.0	0.10	0.10	7.0	2,000	14,000	7.48
0.010	1.0	0.10	0.10	25.00	200	5,000	4.52
0.010	1.0	0.10	0.10	25.00	400	10,000	6.31
0.010	1.0	0.10	0.10	100.00	50	5,000	4.52

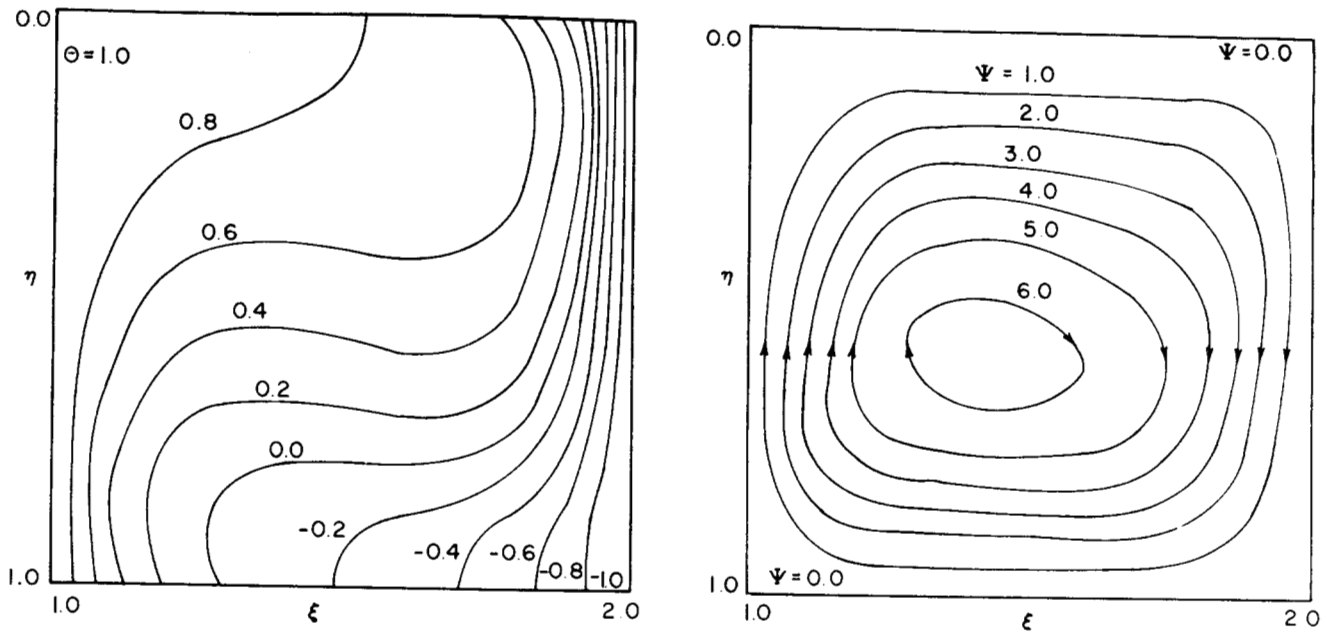

Fig. 3. Steady state isotherms and streamlines—$H/(R_2 - R_1) = 1.0$; $N_{PR} = 1.0$; $N_{GR} = 10{,}000$; $\Delta\xi = \Delta\eta = 1/20$.

The steady-state mean Nusselt number is a good indicator of space convergence with grid spacing. For N_{Ra} values of 1×10^4 and 5×10^4, refinement of the grid spacing from 1/10 to 1/20 gave differences of 23.2 and 28.7%, respectively. The percent differences found for $N_{\overline{Nu}}$ raise some doubts about the validity of computer-generated rates of heat transfer. A great many finite-difference approximations are available which can be used to represent the boundary flux in Equation (10). Aziz and Hellums used a second-order correct three-point formula in their studies; Samuels and Wilkes have used third-order four-point formulas. The percent differences in $N_{\overline{Nu}}$ obtained upon refinement of the numerical grid in this study are of the same order of magnitude as those obtained by other investigators.

Variation of $N_{\overline{Nu}}$ with N_{Pr}, N_{Ra}, $H/(R_2 - R_1)$

The variation of $N_{\overline{Nu}}$ with N_{Ra} and N_{Pr} for $H/(R_2 - R_1) = 1.0$ and $\Delta\xi = \Delta\eta = 1/10$, is shown in Table 2. As expected, $N_{\overline{Nu}}$ increases with increasing N_{Ra}, but a definite Prandtl number dependence is indicated. Many more computer runs are needed before any definite correlations can be obtained.

The dependence of the Nusselt number on geometrical ratios, as indicated in Table 1, is indefinite. Because of the large number of grid points needed to characterize the $H/(R_2 - R_1) = 0.5$, 2.0, and 3.0 cases, the computer time required to make a thorough investigation of the effects of geometry on $N_{\overline{Nu}}$ could not be justified.

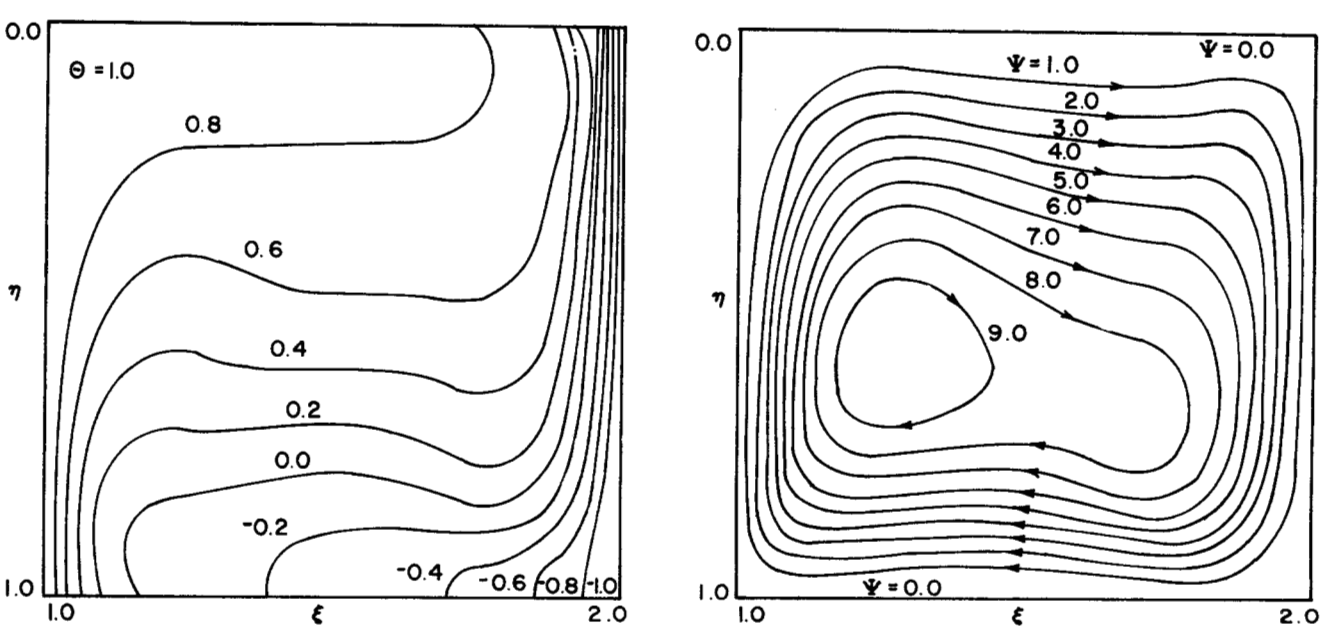

Fig. 4. Steady state isotherms and streamlines—$H/(R_2 - R_1) = 1.0$; $N_{PR} = 1.0$; $N_{GR} = 50{,}000$; $\Delta\xi = \Delta\eta = 1/20$.

Interpretation of Isotherm and Streamline Plots

The condition of pure conduction and no fluid motion exists when the buoyant and viscous forces in the fluid are completely in balance and when heat is transferred solely by diffusional processes. The temperature gradient across the cavity is horizontal with the conduction profiles being vertical lines traversing the entire length of the cavity. When N_{Ra} approaches 10^3, large temperature gradients grow near the vertical walls giving rise to the formation of thermal boundary layers and fluid velocities sufficient to form hydrodynamic boundary layers. A unicellular flow pattern is generated in the enclosure.

When $N_{Ra} \geq 5 \times 10^3$, a fully developed boundary-layer flow exists in the cavity. This flow is similar to that near a heated vertical plate except that, in the cavity, two boundary layers are competing for the fluid.

The interaction of the boundary layers on the vertical walls leads to a nearly uniform vertical temperature gradient in the core of the annulus. The interior region of the annulus is thus characterized by horizontal, regularly spaced isotherms—the region is thermally stratified. The streamlines in the central portion of the cavity are also found to be nearly horizontal.

In the case where $H/(R_2 - R_1) = 3.0$ as shown in Figure 5, a pronounced boundary-layer flow has already developed within the cavity. The isotherms exhibit a considerable amount of distortion from the vertical conduction profile and a single convective cell exists in the cavity.

ACKNOWLEDGMENT

The authors thank the National Science Foundation, whose financial support made this work possible, and the Marathon Oil Corp., Findlay, Ohio, and Owens-Illinois, Inc., Toledo, Ohio, for the use of their computer facilities. Thanks are also due to Mr. Darel Eschbach, Director of the University of Toledo Computation Center.

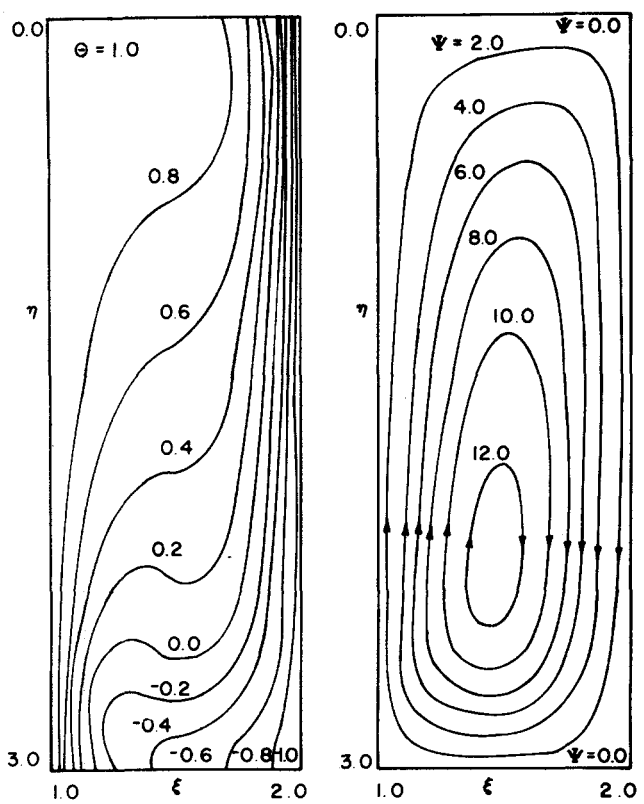

Fig. 5. Steady state isotherms and streamlines—$H/(R_2 - R_1) = 3.0$; $N_{PR} = 1.0$; $N_{GR} = 5{,}000$; $\Delta\xi = \Delta\eta = 1/10$.

TABLE 2. VARIATION OF $N_{\overline{Nu}}$ WITH N_{Pr} FOR SELECTED N_{Ra} WITH $H/(R_2 - R_1) = 1.0$ AND GRID SPACING OF 1/10

$N_{Ra} = 5{,}000$		$N_{Ra} = 10{,}000$	
N_{Pr}	$N_{\overline{Nu}}$	N_{Pr}	$N_{\overline{Nu}}$
0.73	4.43	0.73	6.13
1.00	4.46	1.00	6.17
7.00	4.50	7.00	6.36
25.00	4.52	25.00	6.31
100.00	4.52	—	—

NOTATION

C_p = heat capacity at constant pressure
g = acceleration of gravity
h = local heat transfer coefficient
H = height of annular container
k = thermal conductivity of fluid
L = characteristic length
N_{Gr} = $g\beta(T_1 - T_2)(R_2 - R_1)^3/2\nu_0^2$, Grashof number
$N_{\overline{Nu}}$ = hL/k, Nusselt number
N_{Pr} = $C_p\mu/k = \nu/\alpha$, Prandtl number
N_{Ra} = $N_{Gr} \cdot N_{Pr}$, Rayleigh number
p' = fluid pressure deviation
P = $p'(R_2 - R_1)^2/\rho_0\nu_0^2$, dimensionless pressure deviation
r = radial coordinate
R_1 = radius of inner cylinder
R_2 = radius of outer cylinder
t = time
T = fluid temperature
U = $v_r(R_2 - R_1)/\nu_0$, dimensionless radial velocity component
v_r = radial component of fluid velocity vector
v_z = axial component of fluid velocity vector
V = $v_z(R_2 - R_1)/\nu_0$, dimensionless axial velocity component
z = axial coordinate

Greek Letters

α = $k/\rho C_p$, thermal diffusivity
β = thermal coefficient of volume expansion
$\Delta\xi$ = dimensionless space increment between vertical grid lines
$\Delta\eta$ = dimensionless space increment between horizontal grid lines
$\Delta\tau$ = dimensionless time increment
η = $z/(R_2 - R_1)$, dimensional axial coordinate
θ = $2(T - T_0)/(T_1 - T_2)$, dimensionless temperature
μ = coefficient of shear viscosity
ν = kinematic viscosity
ξ = $r/(R_2 - R_1)$, dimensionless radial coordinate
ρ = fluid density
τ = $t\nu_0/(R_2 - R_1)^2$, dimensionless time
Ψ = dimensionless stream function
ω = dimensionless vorticity

Subscripts

0 = evaluated at mean fluid temperature
s = value at bounding surface

Superscripts

~ = conduction value
′ = variation from value at mean fluid temperature

LITERATURE CITED

1. Abbott, M. R., *Quart. J. Mech. Appl. Math.*, **17**, 471 (1964).
2. Aziz, K., and J. D. Hellums, *Phys. Fluids*, **10**, 314 (1967).
3. Brian, P. L. T., *AIChE J.*, **7**, 367 (1961).
4. Deardorff, J. W., *J. Atmos. Sci.*, **21**, 419 (1964).
5. Douglas, J., Jr., *Num. Math.*, **4**, 41 (1962).
6. Elder, J. W., *J. Fluid Mech.*, **24**, 823 (1966).
7. Fromm, J. E., *Phys. Fluids*, **8**, 1757 (1965).
8. Hellums, J. D., Ph.D. thesis, Univ. Michigan, Ann Arbor (1963).
9. Lemlich, R., and L. Crawford, *Ind. Eng. Chem. Fundamentals*, **1**, 260 (1962).
10. Liu, C. Y., W. K. Mueller, and F. Landis, *Intern. Develop. Heat Transfer*, Part IV, 976 (1961).
11. Noble, J. J., Ph.D. thesis, Massachusetts Inst. Technol., Cambridge (1968).
12. Piacsek, S. A., Ph.D. thesis, Massachusetts Inst. Technol., Cambridge (1968).
13. Samuels, M. R., Ph.D. thesis, Univ. Michigan, Ann Arbor (1965).
14. ———, *Phys. Fluids*, **11**, 1889 (1968).
15. Schwab, T. H., M.S. thesis, Univ. Toledo, Ohio (1968).
16. Wilkes, J. D., Ph.D. thesis, Univ. Michigan, Ann Arbor (1963).
17. Williams, G. P., *J. Atmos. Sci.*, **24**, Part 1, 144 (1967).
18. ———, *ibid.*, Part 2, 162 (1967).

Manuscript received October 10, 1968; revision received April 14, 1969; paper accepted April 16, 1969.

Numerical Treatment of Fully Developed Laminar Flow in Helically Coiled Tubes

L. C. TRUESDELL, JR., and R. J. ADLER
Case Western Reserve University, Cleveland, Ohio

Laminar flow in helically coiled tubes is treated numerically. Fully developed axial and secondary velocities are calculated for both circular and elliptical cross sections. Only closely wrapped helices, that is, helices with modest pitch, are considered. Ten solutions with Deans numbers up to 200 have good accuracy. Two additional solutions with Deans numbers up to 280 are approximate.

Secondary flow, that is, flow perpendicular to the main direction of flow, occurs whenever fluid passes through a curved tube or channel. The phenomenon is caused by centrifugal forces, and can be readily explained by reference to Figure 1, the cross section of a helically coiled tube. Near the tube's center the axial velocity is greatest, causing centrifugal forces to act most strongly. Fluid is thrown outward and replaced by recirculating fluid which flows inward along the walls. In laminar and turbulent flow two strong symmetrical patterns are normally established.

Certain important effects are caused by secondary flow. For example, the snaking or meandering of rivers flowing across alluvial plains is due to secondary flow (*1, 2*). Superior heat transfer characteristics are possessed by coiled tube heat exchangers (*3* to *5*). Secondary flow stabilizes laminar flow, transition Reynolds numbers of 6,000 to 8,000 being characteristic of helically coiled tubes (*6*). Secondary flow markedly reduces axial dispersion, an effect of interest in chromatography and chemical reactor design (*7*). These effects and others are described in a literature which dates back almost 100 yr. A listing of important references through 1964 has been compiled (*7*).

A numerical treatment of fully developed laminar flow, including secondary flow, is reported here for helically coiled tubes. The treatment is based on a finite-difference approximation to the governing continuous equations and is valid over a greater range of operating conditions than previous analytical solutions (*8* to *11*). Analytical solutions to date have been limited because they are based on expressing velocity and pressure in a power series in a/r, where a is the radius of the tube and r is the radius of curvature of the helix. Because of algebraic complexity, it has been practical to retain only terms of first order. The resulting analytical solutions have been valid only for small values, perhaps up to two or three, of a dimensionless criterion called the Deans number, $N_{Re}(a/r)^{1/2}$. Numerical solutions having good accuracy are presented in this paper for Deans numbers up to approximately 200.

The work reported encompasses both round and elliptical cross sections. Incompressible, fully developed flow is assumed. Only the practically important case of small pitch $h/2\pi r$ is considered (see Figure 2 for the definition of h).

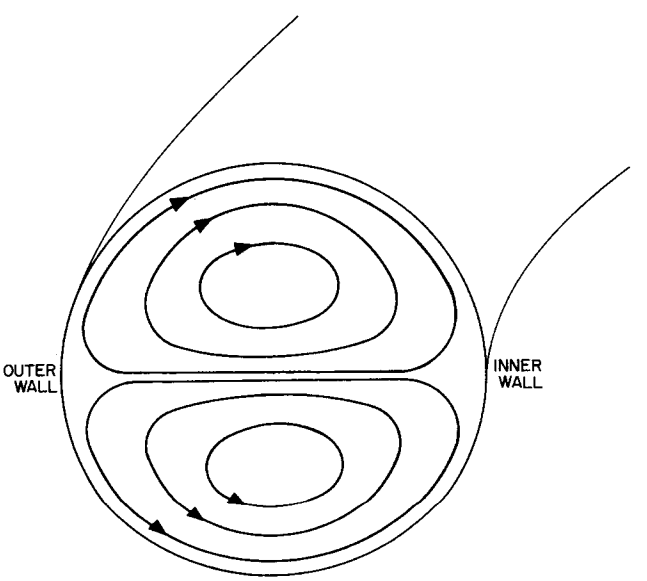

Fig. 1. Secondary flow patterns in the cross section of a helically coiled tube.

L. C. Truesdell, Jr., is with Shell Development Company, Emeryville, California.